iScience

CellPress OPEN ACCESS

Article

Gene expression of non-homologous end-joining pathways in the prognosis of ovarian cancer

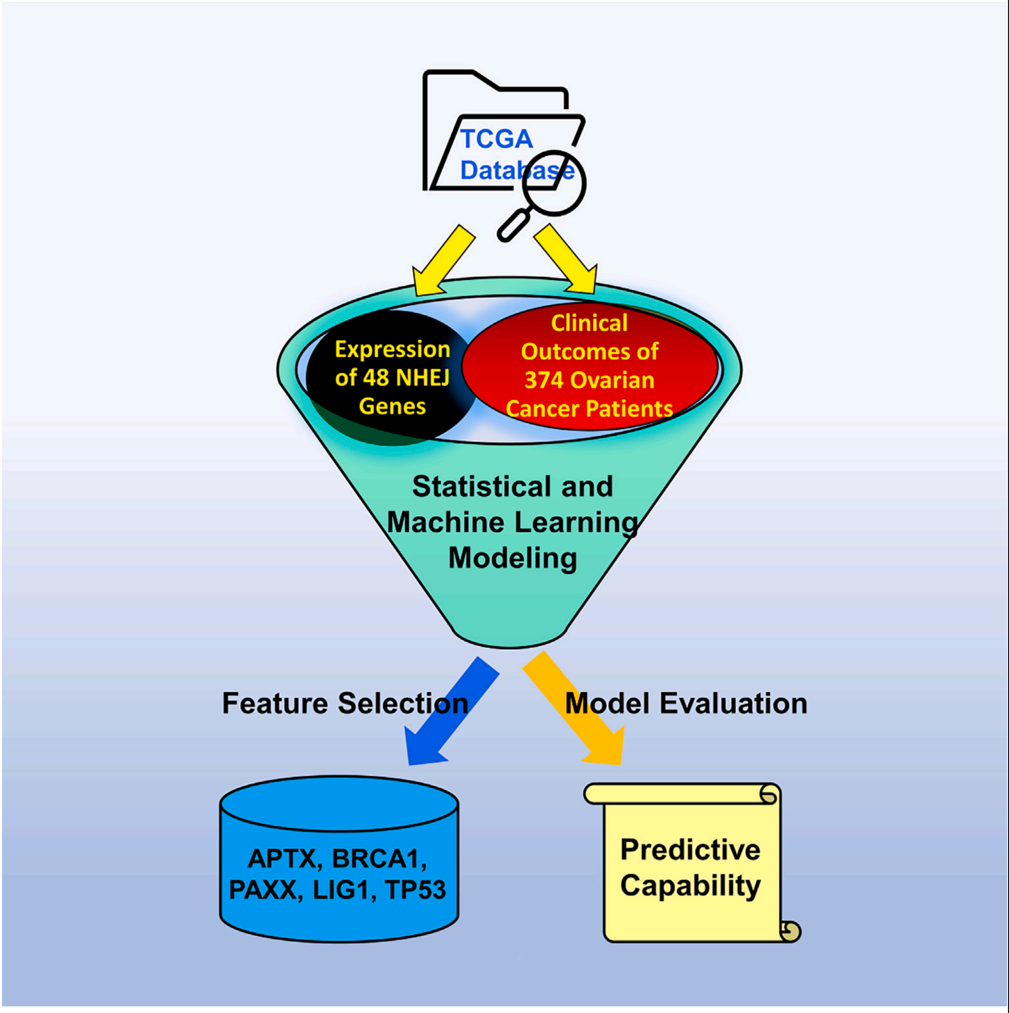
TCGA Database
Expression of 48 NHEJ Genes
Clinical Outcomes of 374 Ovarian Cancer Patients
Statistical and Machine Learning Modeling
Feature Selection
Model Evaluation
APTX, BRCA1, PAXX, LIG1, TP53
Predictive Capability

Ethan S. Lavi, Z. Ping Lin, Elena S. Ratner

z.ping.lin@yale.edu (Z.P.L.)
elena.ratner@yale.edu (E.S.R.)

Highlights

NHEJ gene expression can be used as biomarkers of prognosis in ovarian cancer

APTX, *BRCA1*, *PAXX*, *LIG1*, and *TP53* were identified as the most impactful genes

A higher quality and quantity of data are required to train complex prediction models

Lavi et al., iScience *26*, 107934
October 20, 2023 © 2023 The Author(s).
https://doi.org/10.1016/j.isci.2023.107934

iScience

CellPress OPEN ACCESS

Article

Gene expression of non-homologous end-joining pathways in the prognosis of ovarian cancer

Ethan S. Lavi,[1] Z. Ping Lin,[1,2,*] and Elena S. Ratner[1,*]

SUMMARY

Ovarian cancer is the deadliest gynecologic malignancy in women, with a 46% five-year overall survival rate. The objective of the study was to investigate the effects of non-homologous end-joining (NHEJ) genes on clinical outcomes of ovarian cancer patients. To determine if these genes act as prognostic biomarkers of mortality and disease progression, the expression profiles of 48 NHEJ-associated genes were analyzed using an array of statistical and machine learning techniques: logistic regression models, decision trees, naive-Bayes, two sample t-tests, support vector machines, hierarchical clustering, principal component analysis, and neural networks. In this process, the correlation of genes with patient survival and disease progression and recurrence was noted. Also, multiple features from the gene set were found to have significant predictive capabilities. *APTX*, *BRCA1*, *PAXX*, *LIG1*, and *TP53* were identified as most important out of all the candidate genes for predicting clinical outcomes of ovarian cancer patients.

INTRODUCTION

Cells are constantly monitoring for any DNA damage caused by environmental insults or incurred during DNA replication. When identified, multiple DNA repair pathways can be employed to repair the abnormality. The most lethal type of DNA damage, DNA double-strand break (DSB), is repaired by the error-free homologous recombination (HR) pathway or the error-prone non-homologous end-joining (NHEJ) pathway.[1] DNA damage that starts as a single-strand break (SSB) is repaired mainly using poly ADP-ribose polymerase (PARP) through the process of base excision repair.[2] If the SSB is left unrepaired, it can progress to a DSB, which is usually repaired through the HR pathway. When this pathway is unavailable, cells resort to the NHEJ pathway.[3] In cancer cells with HR deficiency, the use of a PARP inhibitor leaves the cancer cells with the NHEJ pathway as the only option for repairing DSBs.[4,5] It is postulated that when cells use the NHEJ repair mechanism, it leads to deleterious mutations or chromosomal abnormalities that promote cell death.[6] Thus, many cancers, such as ovarian and breast cancers with defective HR repair, are susceptible to the cytotoxicity of PARP inhibitors through synthetic lethality. However, NHEJ repair could also act as a double-edged sword. Using this error-prone repair mechanism, surviving cancer cells can acquire advantageous mutations that lead to resistance to therapy.[7]

The NHEJ pathway can be further divided to two sub-pathways: classical or canonical NHEJ (cNHEJ) and alternative NHEJ (altNHEJ). cNHEJ involves the direct rejoining and ligation of two broken ends of a DSB. This process often leads to a small insertion or deletion (1–5 bp) at the break point. By contrast, altNHEJ requires additional end resection of both ends to generate a small microhomology sequence for pairing and joining. This process can result in a large insertion or deletion at the repaired junction. In mammalian cells, cNHEJ evolves to serve as a predominant mechanism to repair DSBs throughout the cell cycle and maintain genomic stability.[6] altNHEJ functions as a backup repair mechanism when critical components for cNHEJ and HR pathways are unavailable. Therefore, the error-prone and mutagenic nature of NHEJ may be mainly attributable to altNHEJ.[3] If NHEJ is not available, single strand annealing (SSA) is last in the hierarchy, being the most mutagenic.[8] SSA is treated as an alternative to altNHEJ, specifically geared toward repairing resected DSBs in the S/G2 phase of the cell.[9]

The connections between genes involved in NHEJ and ovarian cancer outcomes remain largely unknown. However, the involvement of NHEJ pathways in cell death and mutagenic processes implies that these genes may serve as a biomarker of cancer mortality. Furthermore, the levels of NHEJ gene expression quantify the activity of the DNA repair process and potentially provide an indicator of the cancer cell's fate in response to treatment.[10] Thus, a mathematical model that correlates these genes with cancer mortality may hold promise to predict treatment and survival outcomes in patients. However, complex problems such as this may require a sophisticated model.

There are many genes involved in the NHEJ mechanism. Of them, 48 of the most prominent genes related to DNA repair, with relationships with NHEJ, were chosen for investigation. In early experimentation, classic statistical techniques were unable to check for intricate relationships with prognosis. As such, a stronger method was desired to thoroughly analyze these genes to predict prognosis. As opposed to classical methods, deep learning is a novel approach that has rapidly improved the success of models by leveraging large amounts of data to learn difficult patterns. For this approach, a neural network model was created. A subset of the data is used to train and tune the network's

[1]Department of Obstetrics, Gynecology, and Reproductive Sciences, Yale University School of Medicine, New Haven, CT 06510, USA
[2]Lead contact
*Correspondence: z.ping.lin@yale.edu (Z.P.L.), elena.ratner@yale.edu (E.S.R.)

https://doi.org/10.1016/j.isci.2023.107934

Table 1. Logistic regression of 48 genes to survival outcome conducted on the ovarian cancer dataset

Gene	Estimate	Std. Error	t value	Pr(>|t|)
TP53BP1	**−0.077836**	**0.041337**	**−1.883**	**0.0606**
RAD52	**−0.063386**	**0.032482**	**−1.951**	**0.0519**
MRE11	−0.061275	0.039049	−1.569	0.1176
POLQ	−0.058071	0.049820	−1.166	0.2446
XRCC5	−0.056447	0.037277	−1.514	0.1309
XRCC1	−0.047599	0.036273	−1.312	0.1904
XRCC7	−0.037603	0.041710	−0.902	0.3680
MSH6	−0.034452	0.062775	−0.549	0.5835
EXD2	−0.027621	0.034477	−0.801	0.4236
RBBP8	−0.020403	0.029359	−0.695	0.4876
APLF	−0.019839	0.033619	−0.590	0.5555
RIF1	−0.016524	0.039430	−0.419	0.6754
LIG4	−0.013188	0.031801	−0.415	0.6786
EXO1	−0.010461	0.051082	−0.205	0.8379
PAXX	−0.008699	0.033950	−0.256	0.7979
H2AX	−0.007304	0.035200	−0.208	0.8357
XRCC6	−0.006841	0.033174	−0.206	0.8367
PNKP	−0.005799	0.038298	−0.151	0.8797
LIG3	−0.003759	0.028825	−0.130	0.8963
BRCA1	−0.002899	0.038271	−0.076	0.9397
RAD1	−0.002605	0.034548	−0.075	0.9399
ERCC1	0.001512	0.036701	0.041	0.9672
RAD50	0.003361	0.033791	0.099	0.9208
NBN	0.005523	0.031675	0.174	0.8617
ATR	0.006529	0.041340	0.158	0.8746
MSH3	0.008567	0.041481	0.207	0.8365
RPA1	0.010596	0.032621	0.325	0.7455
XRCC4	0.013539	0.036136	0.375	0.7082
RAD51	0.018338	0.039797	0.461	0.6452
TP53	0.018412	0.028813	0.639	0.5233
MLH1	0.023919	0.035277	0.678	0.4982
ERCC4	0.024449	0.031275	0.782	0.4349
WRN	0.024710	0.034415	0.718	0.4733
DCLRE1C	0.026012	0.035011	0.743	0.4580
NHEJ1	0.026084	0.036593	0.713	0.4765
PARP1	0.031145	0.042478	0.733	0.4640
PARP3	0.033195	0.031000	1.071	0.2850
POLM	0.033783	0.032540	1.038	0.2999
MLH3	0.036035	0.034967	1.031	0.3035
LIG1	0.036274	0.043006	0.843	0.3996
TDP1	0.040557	0.036737	1.104	0.2704
MSH2	0.043464	0.063100	0.689	0.4914
POLL	0.045968	0.031495	1.460	0.1454
PMS1	**0.052444**	**0.030650**	**1.711**	**0.0880**
CTBP1	**0.052678**	**0.030728**	**1.714**	**0.0874**

(*Continued on next page*)

Table 1. *Continued*

Gene	Estimate	Std. Error	t value	Pr(>|t|)
ATM	0.056676	0.044617	1.270	0.2049
APTX	**0.058779**	**0.031894**	**1.843**	**0.0662**
BRCA2	0.060350	0.039121	1.543	0.1239

Logistic regression for the gene dataset was conducted and each gene was ordered by the estimates. Positive estimates of gene expression are associated with improved survival whereas the negative estimates contribute to poor survival probability. Standard error, a t-value, and a p value for each gene in the logistic regression model was generated. P-values under 0.1 were bolded.

parameters. Then, the model is evaluated on the remaining "testing" set of data.[11] With that in mind, a major contributor to creating a successful deep learning model includes a large dataset size or data augmentation. The latter helps the model from overfitting and achieve higher accuracy by artificially increasing the amount of training data available.[12] Due to the similarity of breast cancer to ovarian cancer, as shown by clinical responses to PARP inhibitors,[13] breast cancer data were included in the training dataset for the deep learning approach.

RESULTS

Linear regression shows *APTX, RAD52, TP53BP1,* and *PMS1* correlate with survival

Linear regression was conducted to take a classic statistical approach to modeling patient' survival. The model attempted to predict the length of survival as a function of the 48 gene expressions. The results produced an estimate, standard error, a t-value, and a p value. RAD52 and TP53BP1 were noted to be significant ($p < 0.05$) and negatively correlated with survival. APTX and PMS1 were also significant at a higher alpha level ($p < 0.1$) and positively correlated (Table S1). However, the mean squared error (MSE) for this model, 692.975, was higher than the control MSE of predicting average survival, 591.318, implying it was not making strong predictions.

Logistic regression identifies *APTX, RAD52, TP53BP1, PMS1,* and *CTBP1* as predictors of survival

Logistic regression was conducted to supplement the results of the linear regression. The analysis produced an estimate, standard error, a t-value, and p value. *RAD52, TP53BP1, CTBP1, PMS1,* and *APTX* were statistically significant ($p < 0.1$). Of those genes, *RAD52* and *TP53BP1* were negatively correlated with survival and *APTX, PMS1,* and *CTBP1* were positively correlated (Table 1). All the other genes gave no indication of their true relationship with patients' survival. In addition, the balanced accuracy of the model was 0.5000, which implies this model was not effective.

Logistic regression identifies *BRCA1, BRCA2, PAXX,* and *DCLRE1C* as predictors of progression

Logistic regression was conducted to assess gene correlation and predictive capabilities on progression. The analysis produced an estimate, standard error, a t-value, and p value. *BRCA1* ($p < 0.01$), *BRCA2* ($p < 0.1$), *PAXX* ($p < 0.05$), and *DCLRE1C* ($p < 0.05$) were statistically significant. Of those genes, *BRCA1, BRCA2* and *PAXX* were negatively correlated with progression and just *DCLRE1C* was positively correlated (Table 2). Similar to survival, using just the statistically significant genes, the balanced accuracy of the model was still low at 0.5185.

Logistic regression demonstrates strong predictive capabilities of recurrence using *MLH3, BRCA2, LIG1, H2AX, TP53, NBN, MLH1,* and *RAD52*

Logistic regression was conducted to assess gene correlation and predictive capabilities on recurrence. The analysis produced an estimate, standard error, a t-value, and p value. *MLH3* ($p < 0.01$), *BRCA2* ($p < 0.005$), and *LIG1* ($p < 0.1$) were statistically significant and negatively correlated with recurrence. In addition, *H2AX* ($p < 0.1$), *TP53* ($p < 0.05$), *NBN* ($p < 0.05$), *MLH1* ($p < 0.05$), and *RAD52* ($p < 0.01$) were statistically significant and positively correlated (Table 3). Using just the statistically significant genes resulted in a balanced accuracy of 0.6397.

T-test identifies genes correlating with prognosis

To further analyze genes using classic statistical methods, two-sample t-tests were conducted. P-values and a correlation indication were generated for each gene and outcome. Among the survival outcome, *DCLRE1C* ($p < 0.05$), *TDP1* ($p < 0.05$), *PARP3* ($p < 0.05$), *APTX* ($p < 0.05$), and *PMS1* ($p < 0.05$), were positively correlated. In the progression outcome, *MRE11* ($p < 0.05$) was positively correlated while *PAXX* ($p < 0.005$) was negatively correlated. Finally, *NBN* ($p < 0.05$), *ATM* ($p < 0.05$), *TP53* ($p < 0.05$), and *MLH1* ($p < 0.05$) were positively correlated and *BRCA2* ($p < 0.05$), *PNKP* ($p < 0.05$), and *PAXX* ($p < 0.05$) were negatively correlated with recurrence (Table 4).

Hierarchical clustering forms a gene cluster with the survival outcome

A dendrogram was generated to visualize the results of the hierarchical clustering analysis. The results showed that *APTX*, *RAD1*, *RBBP8*, *MLH1*, *XRCC6*, *NBN*, *ERCC4*, *LIG3*, and *CTBP1* were part of the same cluster (yellow) with the survival variable (Figure 1). In addition, the hierarchical clustering analysis produced a heatmap that plots correlations between gene variables and patients. In this graph, there were some

Table 2. Logistic regression of 48 genes to progression outcome conducted on the ovarian cancer dataset

Gene	Estimate	Std. Error	t value	Pr(>|t|)
BRCA1	**−0.1242976**	**0.0415754**	**−2.990**	**0.00305**
BRCA2	**−0.0736006**	**0.0416912**	**−1.765**	**0.07862**
PAXX	**−0.0706452**	**0.0331574**	**−2.131**	**0.03402**
MSH6	−0.0648559	0.0648274	−1.000	0.31798
ATM	−0.0619214	0.0476275	−1.300	0.19466
XRCC1	−0.0504561	0.0372236	−1.355	0.17638
PNKP	−0.0449848	0.0397142	−1.133	0.25833
APLF	−0.0350988	0.0338855	−1.036	0.30121
LIG4	−0.0297795	0.0345028	−0.863	0.38884
EXO1	−0.0269956	0.0535367	−0.504	0.61450
PMS1	−0.0265631	0.0303097	−0.876	0.38159
TDP1	−0.0263480	0.0394532	−0.668	0.50481
EXD2	−0.0254016	0.0368288	−0.690	0.49096
XRCC6	−0.0240855	0.0349407	−0.689	0.49121
XRCC5	−0.0228620	0.0371049	−0.616	0.53831
APTX	−0.0191056	0.0345156	−0.554	0.58035
NBN	−0.0186892	0.0318944	−0.586	0.55838
POLM	−0.0180680	0.0331872	−0.544	0.58659
RAD52	−0.0141432	0.0420137	−0.337	0.73665
POLQ	−0.0094281	0.0517068	−0.182	0.85545
RAD1	−0.0076254	0.0349897	−0.218	0.82764
MSH3	−0.0064148	0.0422258	−0.152	0.87936
PARP3	−0.0053147	0.0334938	−0.159	0.87404
RPA1	−0.0003987	0.0363523	−0.011	0.99126
TP53	0.0001413	0.0302283	0.005	0.99627
RIF1	0.0006736	0.0413518	0.016	0.98702
XRCC4	0.0022986	0.0381269	0.060	0.95197
RBBP8	0.0040682	0.0298129	0.136	0.89156
NHEJ1	0.0044331	0.0367863	0.121	0.90417
LIG3	0.0103901	0.0705623	0.147	0.88305
LIG1	0.0125968	0.0473550	0.266	0.79043
RAD50	0.0134041	0.0345507	0.388	0.69835
POLL	0.0181209	0.0320230	0.566	0.57195
CTBP1	0.0218878	0.0310270	0.705	0.48113
XRCC7	0.0312191	0.0429683	0.727	0.46812
H2AX	0.0313751	0.0385220	0.814	0.41608
ERCC4	0.0315063	0.0306286	1.029	0.30455
TP53BP1	0.0321815	0.0418084	0.770	0.44212
MSH2	0.0341919	0.0658308	0.519	0.60391
WRN	0.0406368	0.0376392	1.080	0.28126
ATR	0.0408894	0.0450884	0.907	0.36527
ERCC1	0.0438548	0.0381047	1.151	0.25078
MLH3	0.0473954	0.0485356	0.977	0.32968
MRE11	0.0542806	0.0394192	1.377	0.16964
MLH1	0.0570253	0.0371401	1.535	0.12584

(*Continued on next page*)

Table 2. *Continued*

Gene	Estimate	Std. Error	t value	Pr(>|t|)
RAD51	0.0639152	0.0396143	1.613	0.10781
PARP1	0.0670000	0.0436469	1.535	0.12593
DCLRE1C	**0.0916141**	**0.0392333**	**2.335**	**0.02026**

Logistic regression for the gene dataset was conducted and each gene was ordered by the estimates. Positive estimates of gene expression are associated with likelihood for progression whereas the negative estimates contribute to low progression probability. Standard error, a t-value, and a p value for each gene in the logistic regression model was generated. P-values under 0.1 were bolded.

groups of patients with matching brightness, indicating close distance. These similar patients were likely easier to discern via modeling since the row coloring show that the most of them are also grouped by survival outcome (Figure 2).

Dimensionality cannot be reduced with principal component analysis

Principal component analysis (PCA) was performed to assess redundancies in the data and to note relationships between the gene expression data as a whole and survival. According to the scree plot, a significant portion of the data was lost in the principal components. The first five components covered roughly 40% of the data while the entire ten components covered around 60% (Figure 3). As a result, no separation was observed when graphing alive and deceased patients using the first 2 PCA scores (Figure S1). Furthermore, *EXO1*, *POLQ*, *XRCC7*, *TP53BP1*, and *PARP1* had the highest contributions to the principal components (Figure S2).

Forward feature selection optimizes neural network

To create an effective neural network, forward feature selection was conducted to reduce the amount of irrelevant inputs to the model. In addition, feature selection graphs were generated for each outcome, displaying the trend of accuracy as each feature was added. The survival curve reached peak balanced accuracy with four genes, *RBBP8*, *APTX*, *ERCC1*, and *LIG3*, and then decreased after that (Figure 4). The progression curve was best on average after five, using *PAXX*, *LIG1*, *BRCA1*, *MSH2*, and *POLQ*, before it trended downward (Figure 5). The recurrence graph peaked after seven, with *ERCC4*, *XRCC1*, *TP53*, *RIF1*, *LIG3*, *LIG1*, and *APLF*. However, it didn't consistently trend downward like the survival and progression graphs (Figure 6). In each graph, after seven genes, the max accuracy was stagnant, even though other relevant genes were present. This indicates that more data was likely needed to fit the model.

Neural network makes strong predictions but breast cancer data fails to augment dataset

A bar graph was generated to compare the balanced accuracy of the neural network with and without the breast cancer data as training augmentation. Three gene sets were tested: all the genes, the best from the forward feature selection, and the best from the logistic regression feature selection. Using the top three from the forward feature selection, *RBBP8, APTX,* and *ERRC1*, produced the best balanced accuracy for predicting survival at 0.5776. In addition, in all three trials, the breast cancer data lowered the accuracy, indicating that it can't serve as a method for data augmentation (See Figure S3). For predicting progression, the top four from the forward feature selection, *PAXX, LIG1, BRCA1,* and *MSH2* reached a max balanced accuracy of 0.6310. Lastly, a balanced accuracy of 0.5953 was achieved predicting recurrence using the first six genes from the feature selection, *ERCC4*, *XRCC1*, *TP53*, *RIF1*, *LIG3*, and *LIG1.*

NHEJ related genes predicts prognosis using assorted machine learning methods

The optimal model for predicting survival was the support vector machine (SVM) using *TP53BP1, CTBP1, APTX, RAD52,* and *PMS1* as the features with a balanced accuracy of 0.5887. For progression, the neural network performed the best with 0.6310 balanced accuracy using *PAXX, LIG1, BRCA1,* and *MSH2.* Finally, for predicting recurrence, the logistic regression was strongest at 0.6397 balanced accuracy using *BRCA2, LIG1, NBN, RAD52, TP53, H2AX, MLH1,* and *MLH3* (See all model performance in Table S2).

Simulation determines baseline accuracy for significance

Based on the simulation experiment, the 95% percentile of balanced accuracy that can be achieved from a purely randomly generated dataset maxes out at 0.5546, using the decision tree model. The logistic regression, naive-Bayes, and SVM reached 0.5223, 0.5480, and 0.5425 balanced accuracy respectively. Typically, for each model, the average balanced accuracy was 0.5 (+/− 0.05). Lastly, on average, 4.64 genes were found to have significant p-values out of the 48 genes (See Table S3).

Learning curve demonstrates logistic regression as high-bias method

Learning curves were generated for the logistic regression model predicting survival. The curve showed that the model reached its potential with the features given. Yet it was an "under-fit" to the data as the performance was not very strong (Figure 7).

Table 3. Logistic regression of 48 genes to recurrence outcome conducted on the ovarian cancer dataset

Gene	Estimate	Std. Error	t value	Pr(>|t|)
MLH3	**−0.1436620**	**0.0508329**	**−2.826**	**0.00506**
BRCA2	**−0.1229546**	**0.0434042**	**−2.833**	**0.00496**
LIG3	−0.0960805	0.0733806	−1.309	0.19152
LIG1	**−0.0912946**	**0.0479346**	**−1.905**	**0.05789**
MSH3	−0.0576118	0.0442279	−1.303	0.19381
XRCC5	−0.0561888	0.0382077	−1.471	0.14255
RAD51	−0.0554070	0.0411657	−1.346	0.17944
PAXX	−0.0516596	0.0345574	−1.495	0.13610
ERCC4	−0.0406260	0.0504662	−0.805	0.42151
POLM	−0.0379293	0.0343613	−1.104	0.27064
WRN	−0.0337736	0.0395686	−0.854	0.39411
PMS1	−0.0323849	0.0315185	−1.027	0.30510
POLL	−0.0280872	0.0334922	−0.839	0.40242
XRCC7	−0.0236921	0.0450393	−0.526	0.59929
APTX	−0.0219715	0.0355848	−0.617	0.53746
PNKP	−0.0185921	0.0412459	−0.451	0.65252
MSH2	−0.0154689	0.0681421	−0.227	0.82059
RPA1	−0.0019469	0.0380689	−0.051	0.95925
PARP3	−0.0015842	0.0347633	−0.046	0.96369
DCLRE1C	−0.0009017	0.0410132	−0.022	0.98248
ATR	−0.0007959	0.0466153	−0.017	0.98639
RAD1	0.0031648	0.0360723	0.088	0.93015
BRCA1	0.0060448	0.0409094	0.148	0.88264
XRCC6	0.0061608	0.0364277	0.169	0.86583
CTBP1	0.0066763	0.0324354	0.206	0.83707
EXD2	0.0072041	0.0383797	0.188	0.85125
POLQ	0.0114784	0.0533366	0.215	0.82977
APLF	0.0127893	0.0366496	0.349	0.72739
RBBP8	0.0133334	0.0310312	0.430	0.66777
MSH6	0.0185962	0.0675222	0.275	0.78321
LIG4	0.0279871	0.0363777	0.769	0.44235
MRE11	0.0281447	0.0412834	0.682	0.49598
XRCC4	0.0342550	0.0403606	0.849	0.39678
RAD50	0.0374275	0.0363462	1.030	0.30404
NHEJ1	0.0408071	0.0380589	1.072	0.28457
PARP1	0.0414107	0.0448986	0.922	0.35718
RIF1	0.0422092	0.0426535	0.990	0.32325
TP53BP1	0.0426385	0.0435148	0.980	0.32802
ERCC1	0.0475018	0.0399575	1.189	0.23555
XRCC1	0.0490576	0.0404126	1.214	0.22583
TDP1	0.0608796	0.0413757	1.471	0.14234
EXO1	0.0630913	0.0546782	1.154	0.24956
ATM	0.0633327	0.0488009	1.298	0.19546
H2AX	**0.0751909**	**0.0396955**	**1.894**	**0.05926**
TP53	**0.0774415**	**0.0315229**	**2.457**	**0.01465**

(*Continued on next page*)

Table 3. ***Continued***

Gene	Estimate	Std. Error	t value	Pr(>|t|)
NBN	**0.0788570**	**0.0333537**	**2.364**	**0.01877**
MLH1	**0.0867637**	**0.0397749**	**2.181**	**0.03001**
RAD52	**0.1173069**	**0.0437177**	**2.683**	**0.00774**

Logistic regression for the gene dataset was conducted and each gene was ordered by the estimates. Positive estimates of gene expression are associated with likelihood for recurrence whereas the negative estimates contribute to low recurrence probability. Standard error, a t-value, and a p value for each gene in the logistic regression model was generated. P-values under 0.1 were bolded.

Learning curves indicates deep learning methods potentially will improve with more data

Learning curves were generated for the neural network model in predicting survival when training on a different number of genes. The first curve used the top three genes from the forward feature selection. The curve showed optimal training, needing each patient to reach equal balanced accuracy among the training and testing data (Figure 8). The second curve included the top five genes from the feature selection. This iteration demonstrated that increasing the number of features causes an overfit, trending toward more data equalizing the training and testing scores (Figure 9).

DISCUSSION

The machine learning models: logistic regression, decision tree, support vector machines, naive-Bayes, and neural network indicated the predictive capabilities of the genes on survival, progression, and recurrence outcomes. Balanced accuracy was used as the scoring metric because it achieves equal weighting of correct positive and negative predictions. The feature selection effectively improved this metric while also identifying which genes can act as biomarkers of prognosis. Since the models are assessed on unfamiliar examples, the balanced accuracy reliably showed the model's effectiveness and generalization to new data.

Since the sample size is limited, a lower limit of accuracy was calculated to discern a statistically significant result. The simulation demonstrated that 95% of randomly generated datasets would not produce balanced accuracy above the threshold of 0.555. Since the threshold is beaten by our models, such as the SVM predicting survival achieving 0.5887, the accuracy is acceptable. It is statistically improbable for the actual gene expressions used to have shown correlation with prognosis purely by chance in such a sample.

In addition, the simulation confirmed that some genes are expected to be statistically significant in the t-test, purely by chance. This indicates that lone t-test results should be taken with skepticism. Rather, overlapping results with the feature selections are needed to corroborate the relevance of the gene.

This report demonstrated that NHEJ has an impact on the prognosis outcomes of ovarian cancer patients. Through multiple methods of statistical inference, several NHEJ genes that take a leading role in the clinical outcomes of ovarian cancer are identified. Based on the result of the logistic regression, and further supported by the linear regression, *APTX*, *RAD52*, *TP53BP1*, *PMS1*, and *CTBP1* correlate with patients' survival outcomes. The two-sample t-test analysis showed that *DCLRE1C*, *PARP3*, *TDP1*, *APTX*, and *PMS1* likely exhibit significant differences between alive and deceased patients. In the forward feature selection, the genes *RBBP8*, *APTX*, *ERCC1*, and *LIG3* were identified as optimal for predictions. Moreover, our hierarchical clustering analysis revealed that *RBBP8*, *LIG3*, and *APTX* are clustering with survival outcomes, among other genes. Because the scree plot demonstrated that significant information was lost in its dimensionality reduction, the results of the PCA are questionable.

The results for top genes correlated with the survival outcome was presented as a table for clarity (Table 5). One interesting association that was noted was that genes with positive survival outcomes typically promoted cNHEJ and SSA while those with negative survival outcomes promoted altNHEJ. *CTBP1* and *RAD52* were the sole exceptions to this trend. In addition, *TP53BP1* has been supported to have a role in both pathways, so its effect is ambiguous. *PMS1*, *MLH1*, and *RAD52* are also known mismatch repair (MMR) genes,[14] so their involvement in MMR rather than SSA might also be related to this trend. This casual observation is only sufficient for hypothesis generation, requiring further validation.

In predicting progression, the result of the logistic regression showed *BRCA1*, *BRCA2*, *PAXX*, and *DCLRE1C* are correlated. The two-sample t-test analysis corroborated *PAXX*'s relationship with progression and it further added *MRE11*. In the forward feature selection, *BRCA1* and *PAXX* appeared again. In addition to *BRCA1* and *PAXX*, *LIG1*, *MSH2*, and *POLQ* were used to achieve optimal progression predictions with the neural network. The recurrence logistic regression incorporated *BRCA2*, *LIG1*, *H2AX*, *TP53*, *NBN*, *MLH1*, and *RAD52*. The t-test found significance in *BRCA2*, *TP53*, *NBN* and *MLH1* as well and further revealed *PNKP*, *PAXX*, and *ATM* as relevant. Yet the feature selection found *ERCC4*, *XRCC1*, *TP53*, *RIF1*, *LIG3*, and *LIG1* were best for the neural network, the only overlap being *TP53* and *LIG1*.

An interesting thing noted was the neural network and logistic regression didn't have complete overlap in their feature sets with each other and the t-test. This likely indicates that the models could reach higher predictive capabilities by including all the relevant features discovered. It also narrows the upmost critical factors, with *APTX* in survival, *PAXX* and *BRCA1* in progression, and *TP53* and *LIG1* in recurrence being shared by both feature selections conducted.

In the learning curves, the logistic regression model showed a high bias issue indicating that it needs to have more complexity. Transitioning to the neural network, there is a high variance issue, showing that the data became insufficient to train the survival models with at least five

Table 4. Two sample t-tests for survival, progression, and recurrence

Gene	Survival (p)	Survival positive correlation	Progression (p)	Progression positive correlation	Recurrence	Recurrence positive correlation
XRCC6	0.1365	TRUE	0.4762	TRUE	0.1414	TRUE
XRCC5	0.3400	FALSE	0.4559	FALSE	0.3177	TRUE
XRCC7	0.3347	FALSE	0.1218	TRUE	0.2297	TRUE
LIG4	0.3816	TRUE	0.1728	FALSE	0.2789	FALSE
LIG3	0.3274	FALSE	0.2043	TRUE	0.2824	TRUE
LIG1	0.3058	TRUE	0.3732	FALSE	0.1334	FALSE
XRCC4	0.2605	TRUE	0.3199	FALSE	0.4431	TRUE
NHEJ1	0.2924	TRUE	0.0833	TRUE	0.1103	TRUE
XRCC1	0.0599	FALSE	0.1989	FALSE	0.3436	TRUE
DCLRE1C	**0.0209**	**TRUE**	0.0654	TRUE	0.2610	FALSE
TP53BP1	0.2826	FALSE	0.0775	TRUE	0.1005	TRUE
BRCA1	0.3101	TRUE	0.1357	FALSE	0.1996	TRUE
BRCA2	0.1017	TRUE	0.0521	FALSE	**0.0134**	**FALSE**
EXO1	0.1077	TRUE	0.4149	FALSE	0.2766	TRUE
EXD2	0.4229	TRUE	0.3532	TRUE	0.4824	TRUE
POLM	0.2072	TRUE	0.4002	TRUE	0.2672	FALSE
POLL	0.2428	TRUE	0.1369	TRUE	0.2618	TRUE
POLQ	0.2806	TRUE	0.4212	FALSE	0.1701	FALSE
RAD50	0.1986	TRUE	0.0601	TRUE	0.1568	TRUE
MRE11	0.4411	FALSE	**0.0382**	**TRUE**	0.0615	TRUE
NBN	0.2461	TRUE	0.1567	TRUE	**0.0306**	**TRUE**
TDP1	**0.0160**	**TRUE**	0.4932	FALSE	0.4327	TRUE
RBBP8	0.2539	TRUE	0.2660	TRUE	0.1830	TRUE
CTBP1	0.2030	TRUE	0.4875	FALSE	0.4219	TRUE
APLF	0.2423	TRUE	0.4109	FALSE	0.4268	TRUE
PARP1	0.1572	TRUE	0.1688	TRUE	0.1550	TRUE
PARP3	**0.0180**	**TRUE**	0.1810	TRUE	0.3649	TRUE
PNKP	0.4876	TRUE	0.0553	FALSE	**0.0365**	**FALSE**
APTX	**0.0109**	**TRUE**	0.1646	FALSE	0.4179	FALSE
WRN	0.3309	TRUE	0.1074	TRUE	0.2218	FALSE
PAXX	0.3906	TRUE	**0.0010**	**FALSE**	**0.0261**	**FALSE**
RIF1	0.4603	TRUE	0.4129	FALSE	0.4573	TRUE
RAD52	0.0707	FALSE	0.4665	TRUE	0.0502	TRUE
RAD51	0.2935	TRUE	0.2066	TRUE	0.4841	TRUE
ATM	0.3451	TRUE	0.1067	TRUE	**0.0424**	**TRUE**
ATR	0.1619	TRUE	0.1270	TRUE	0.3542	TRUE
TP53	0.2473	TRUE	0.4517	FALSE	**0.0169**	**TRUE**
H2AX	0.3463	FALSE	0.4039	FALSE	0.1224	TRUE
ERCC1	0.1258	FALSE	0.4466	FALSE	0.3870	FALSE
ERCC4	0.2544	TRUE	0.1472	TRUE	0.2574	TRUE
RPA1	0.1940	TRUE	0.3106	TRUE	0.0904	TRUE
MSH2	0.1508	TRUE	0.2731	TRUE	0.1099	TRUE
MSH3	0.1816	TRUE	0.1493	TRUE	0.2319	TRUE
RAD1	0.2231	TRUE	0.2883	FALSE	0.1843	FALSE

(*Continued on next page*)

Table 4. *Continued*

Gene	Survival (p)	Survival positive correlation	Progression (p)	Progression positive correlation	Recurrence	Recurrence positive correlation
MSH6	0.2942	TRUE	0.4480	FALSE	0.0527	TRUE
PMS1	**0.0454**	**TRUE**	0.4965	TRUE	0.4373	FALSE
MLH1	0.0513	TRUE	0.1560	TRUE	**0.0341**	**TRUE**
MLH3	0.0677	TRUE	0.1051	TRUE	0.1437	FALSE

p values were generated for the gene expression variables when compared to survival, progression, and recurrence. The test determines if the mean is different whether the patient has the outcome or not. Any p values below 0.05 were bolded. In addition, the ''Positive Correlation'' columns relate if higher gene expression associates with the survival, progression, or recurrence outcome.

or six genes. We extrapolated from this that more data can potentially increase the accuracy of the model, since it will allow more features to be included. It was theorized that since breast cancer is similar to ovarian cancer, shown by similar response to PARP inhibitors,[13] the model might be able to apply it to its learning process. The incorporation of breast cancer data into the training of our neural network didn't improve the accuracy. As a result, it is critical that efforts are made to increase data from ovarian cancer patients.

It is important to note that all our models disregarded treatment information, demographics, and other indicators of prognosis. This was to ensure all predictive capabilities came from the gene data. But in the future, by including an array of different biomarkers and collecting more clinical data, a predictive model could be created to achieve a higher accuracy.[26] Or, by emulating our methodology, other sets of genes can be analyzed cost-effectively. At the time, only high-grade serous ovarian cancer data were available. In the future, different types should be investigated to determine the generalization of the findings. Finally, NHEJ genes showed evidence through modeling to be able to predict survival, progression, and recurrence. Thus, further inquiry is necessary to assess the genes' role in regard to each outcome.

Limitations of the study

The study was likely limited by the dataset size. Training a deep learning model requires a large number of examples and the learning curves implied that more are needed. More data would improve confidence in the generalization of results to new patients. In addition, there is concern in the reliability of the recurrence and progression factors. These data were inferred from clinical notes, which may be missing

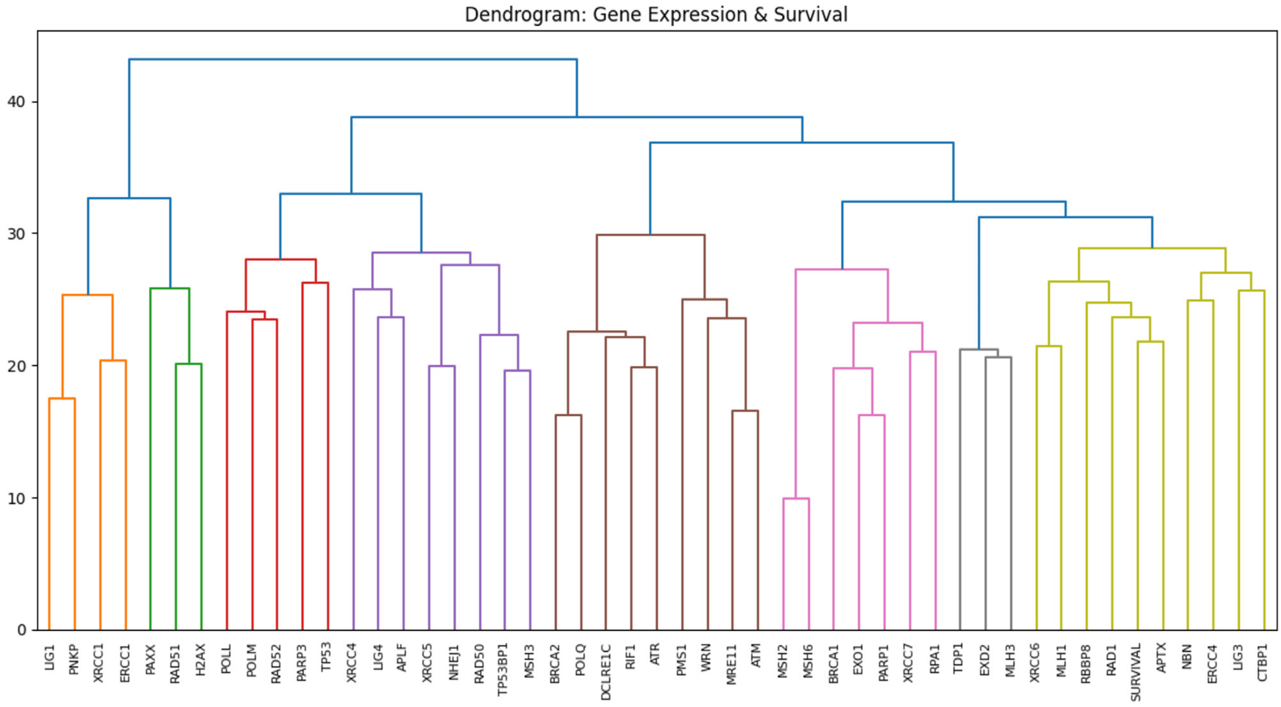

Figure 1. Dendrogram from hierarchical clustering of 48 genes

The dendrogram displays the relatedness between variables. Major clusters are colored on the figure. It is in scale, with lower branches indicating a closer similarity.

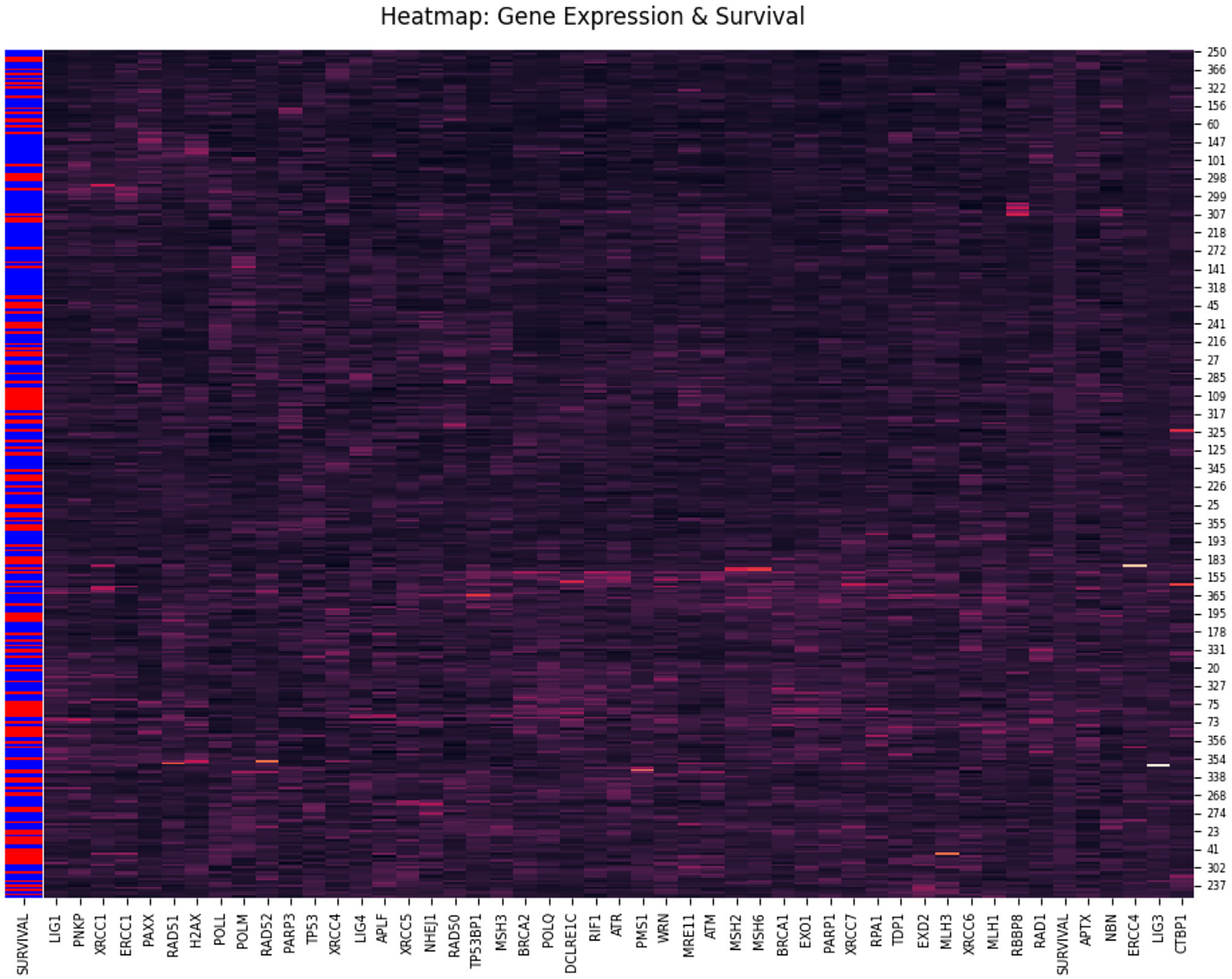

Figure 2. Heatmap from hierarchical clustering of 48 genes

Shows the similarity between gene expression and patients. The brighter the color indicates a higher value, showing where correlation is. The first column are labels for survival, with blue representing deceased and red surviving patients.

information. As a result, recurrence or progression could be mislabeled in the analysis. Lastly, computational strength limited the reliability of the neural network results. Training a deep learning model is stochastic, so the model will not perform the same every time it is trained. To counteract this, the experiment is repeated multiple times, averaging the accuracies to balance the element of randomness. In the forward feature selection, for each gene set, only 30 models total were trained and evaluated. In rare cases, the model group might get lucky in testing, leading to inflated accuracy. Thus, outliers might appear in the result of the forward feature selection. Ideally, each gene set could be tested more thoroughly.

STAR★METHODS

Detailed methods are provided in the online version of this paper and include the following:

- KEY RESOURCES TABLE
- RESOURCE AVAILABILITY
  - Lead contact
  - Materials availability
  - Data and code availability
- EXPERIMENTAL MODEL AND STUDY PARTICIPANT DETAILS
  - Ovarian cancer patients

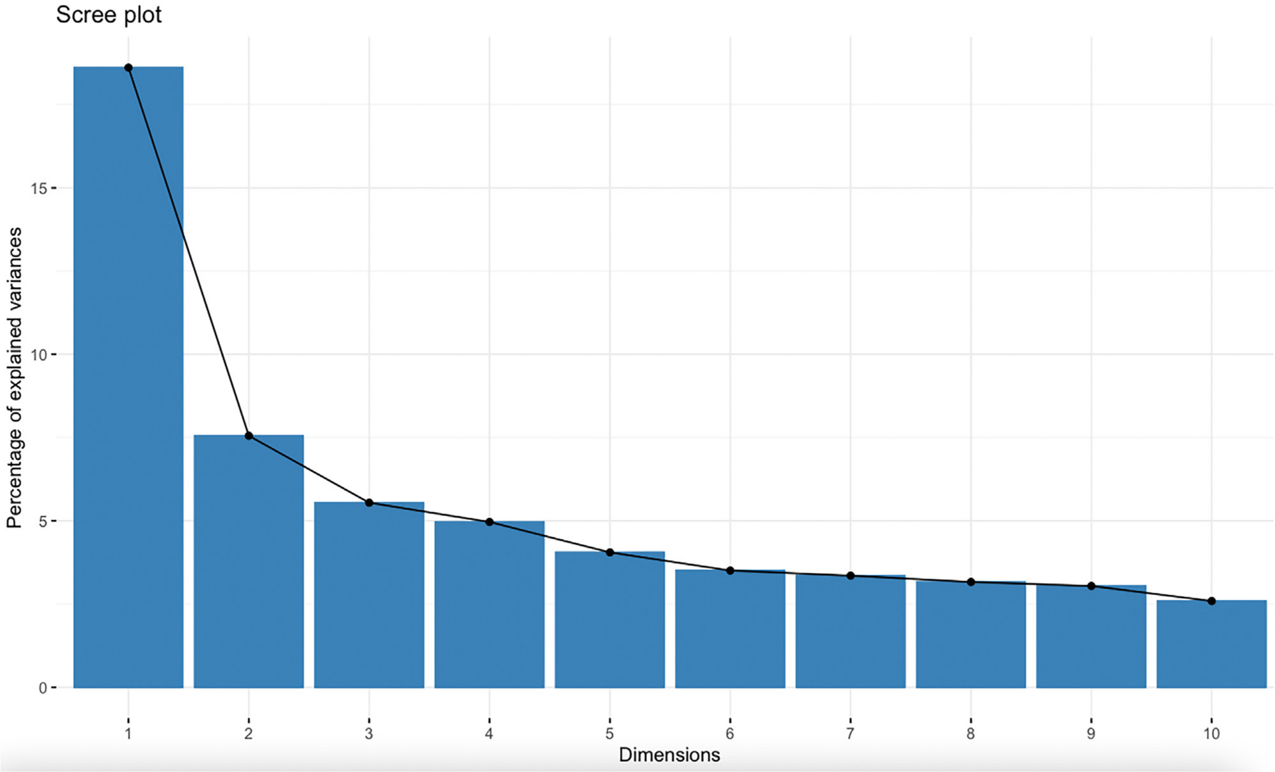

Figure 3. Scree plot for PCA

The scree plot displayed the amount of retained information.

SUPPLEMENTAL INFORMATION

Supplemental information can be found online at https://doi.org/10.1016/j.isci.2023.107934.

ACKNOWLEDGMENTS

The results published here are in whole based upon data generated by the TCGA Research Network: https://www.cancer.gov/tcga. This work was supported by the Discovery to Cure Program at Yale University. Z.P.L. and E.S.R. are Discovery to Cure Fellows. In addition, we thank Catherine Piscitelli, Director of the Amity High School Science Research Program, for her guidance and support throughout the conception and execution of the project.

AUTHOR CONTRIBUTIONS

Conceptualization, Z.P.L.; Methodology, E.S.L.; Software, E.S.L.; Formal Analysis, E.S.L.; Writing – Original Draft, E.S.L.; Writing – Review and Editing, Z.P.L.; Supervision, Z.P.L. and E.S.R.; Project Administration, E.S.R.; Funding Acquisition, E.S.R.

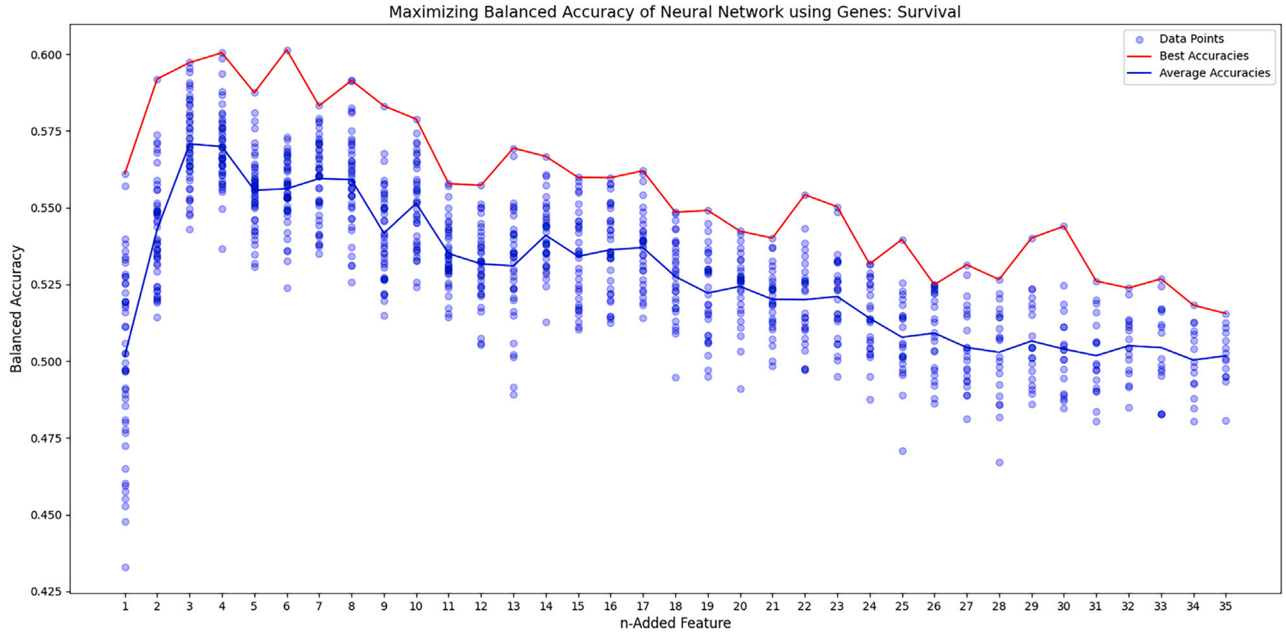

Figure 4. Forward feature selection for survival

The figure graphs the results of the forward feature selection as each gene is added. The blue line is the average of each trial and the red line is the best trial.

DECLARATION OF INTERESTS

The authors declare that they have no competing interest.

Received: February 12, 2023
Revised: April 4, 2023
Accepted: September 13, 2023
Published: September 15, 2023

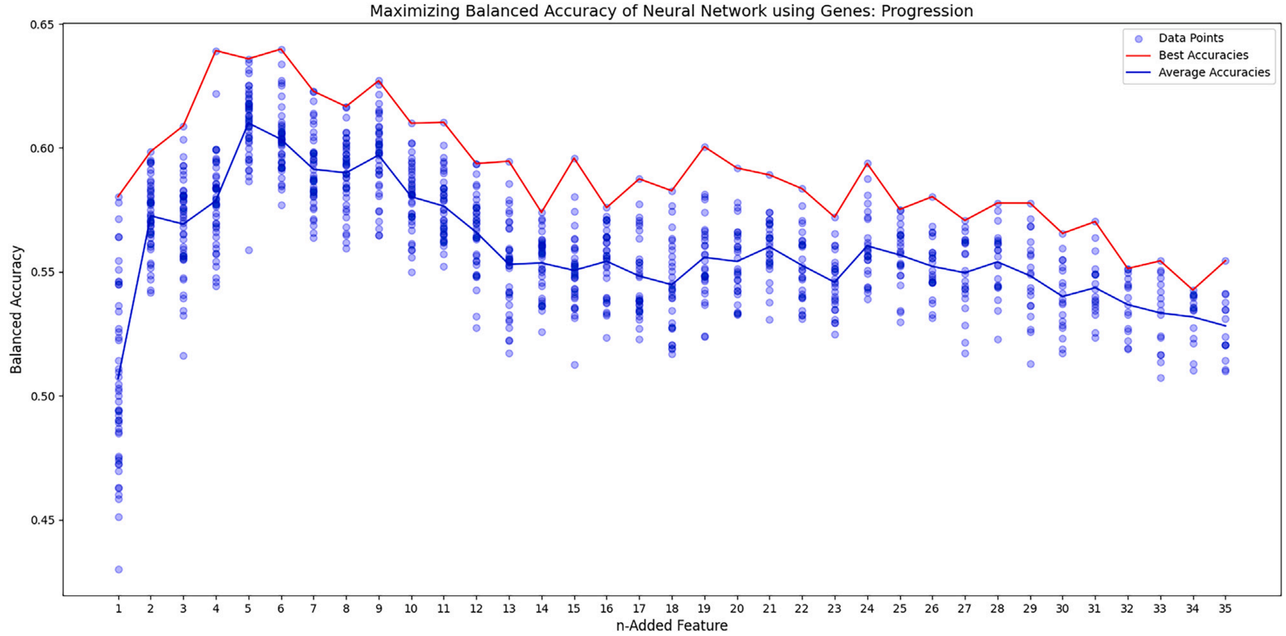

Figure 5. Forward feature selection for progression

The figure graphs the results of the forward feature selection as each gene is added. The blue line is the average of each trial and the red line is the best trial.

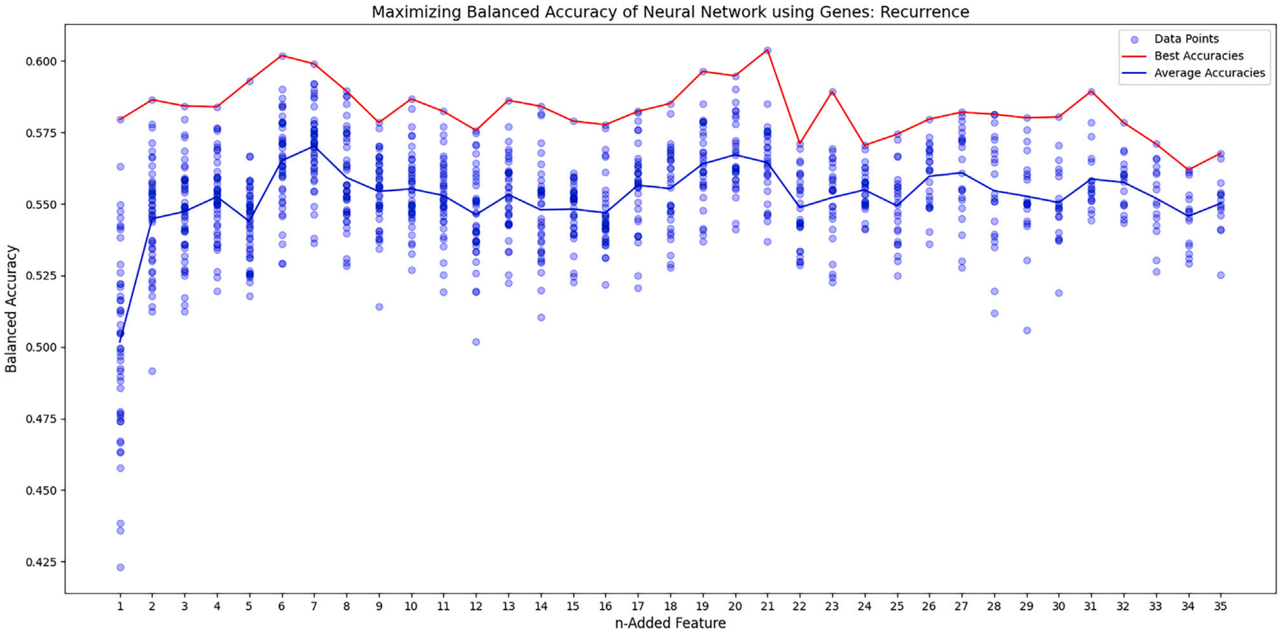

Figure 6. Forward feature selection for recurrence

The figure graphs the results of the forward feature selection as each gene is added. The blue line is the average of each trial and the red line is the best trial.

REFERENCES

1. Vítor, A.C., Huertas, P., Legube, G., and de Almeida, S.F. (2020). Studying DNA Double-Strand Break Repair: An Ever-Growing Toolbox. Front. Mol. Biosci. *7*, 24. https://doi.org/10.3389/fmolb.2020.00024.
2. Davis, A.J., and Chen, D.J. (2013). DNA double strand break repair via non-homologous end-joining. Transl. Cancer Res. *2*, 130–143. https://doi.org/10.3978/j.issn.2218-676X.2013.04.02.
3. Bétermier, M., Bertrand, P., and Lopez, B.S. (2014). Is non-homologous end-joining really an inherently error-prone process? PLoS Genet. *10*, e1004086. https://doi.org/10.1371/journal.pgen.1004086.

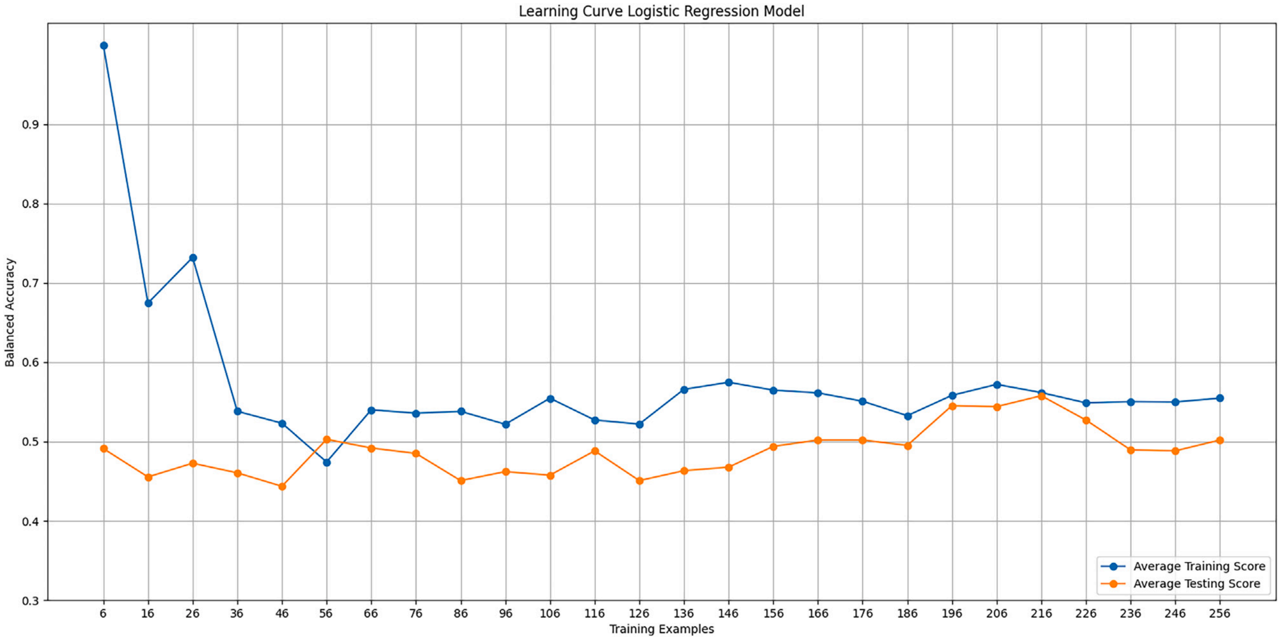

Figure 7. Learning curve, logistic regression model

A learning curve was generated for the logistic regression model. Balanced accuracy evaluated training and testing as a function of the number of training examples. A high training score with few examples is expected since its trivial for the model to fit parameters to only a few data points.

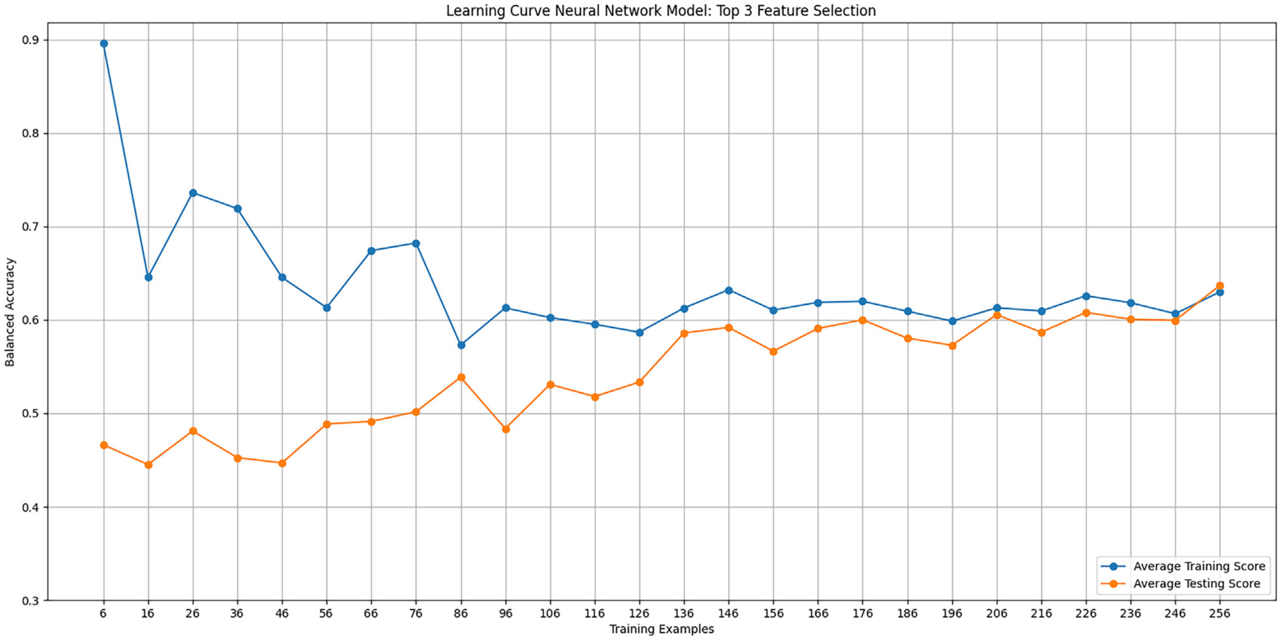

Figure 8. Learning curve, optimal neural network model

A learning curve was generated for the neural network training on the top three genes from the forward feature selection. Balanced accuracy evaluated training and testing as a function of the number of training examples. A high training score with few examples is expected since its trivial for the neural network to fit parameters to only a few data points.

4. Pennington, K.P., Walsh, T., Harrell, M.I., Lee, M.K., Pennil, C.C., Rendi, M.H., Thornton, A., Norquist, B.M., Casadei, S., Nord, A.S., et al. (2014). Germline and somatic mutations in homologous recombination genes predict platinum response and survival in ovarian, fallopian tube, and peritoneal carcinomas. Clin. Cancer Res. *20*, 764–775. https://doi.org/10.1158/1078-0432.CCR-13-2287.

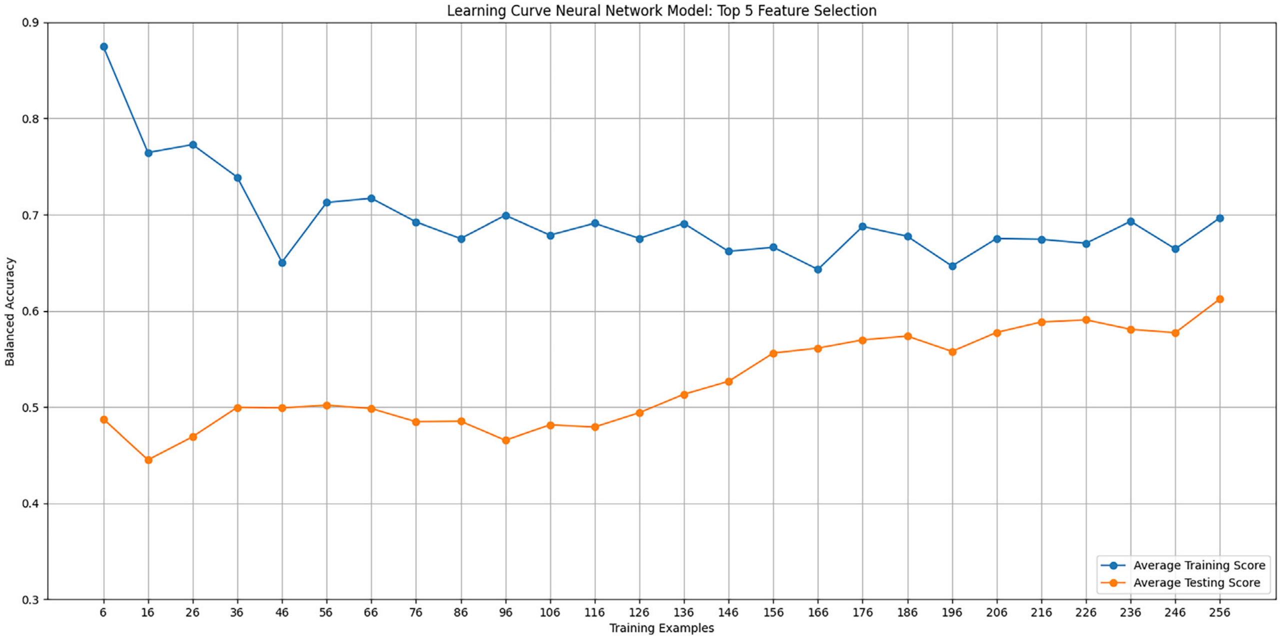

Figure 9. Learning curve, neural network model

A learning curve was generated for the neural network training on the top five genes from the forward feature selection. Balanced accuracy evaluated training and testing as a function of the number of training examples. A high training score with few examples is expected since its trivial for the neural network to fit parameters to only a few data points.

Table 5. Survival gene correlations and role in NHEJ

Gene	Correlation	Analysis	Role in DNA repair	Reference
APTX	Positive	Logistic Regression ($p < 0.1$), T-Test ($p < 0.05$), Forward Feature Selection, Hierarchical Clustering	cNHEJ	Seol et al.[15]; Wang et al.[16]; Chiruvella et al.[17]
DCLRE1C	Positive	T-Test ($p < 0.05$)	cNHEJ	Moscariello et al.[18]; Chiruvella et al.[17]
PARP3	Positive	T-Test ($p < 0.05$)	cNHEJ	Beck et al.[19], Chiruvella et al.[17]
PMS1	Positive	Logistic Regression ($p < 0.1$), T-Test ($p < 0.05$)	SSA	Blasiak[20]
TDP1	Positive	T-Test ($p < 0.05$)	cNHEJ	Chiruvella et al.[17]
CTBP1	Positive	Logistic Regression ($p < 0.1$), Hierarchical Clustering	altNHEJ	Shamanna et al.[21]
MLH1	Positive	Hierarchical Clustering	SSA	Blasiak[20]; Sugawara[22]
TP53BP1	Negative	Logistic Regression ($p < 0.1$)	cNHEJ, altNHEJ	Xiong et al.[23]; Lei[24]
RAD52	Negative	Logistic Regression ($p < 0.1$)	SSA	Stefanovie[25]

A table was compiled to include each gene with a found correlation with survival. The relationship, either positive or negative, was listed along with the analysis it was found in. Finally, the role in NHEJ is listed with its reference.

5. Patel, A.G., Sarkaria, J.N., and Kaufmann, S.H. (2011). Nonhomologous end joining drives poly(ADP-ribose) polymerase (PARP) inhibitor lethality in homologous recombination-deficient cells. Proc. Natl. Acad. Sci. USA *108*, 3406–3411. https://doi.org/10.1073/pnas.1013715108.
6. Rodgers, K., and McVey, M. (2016). Error-Prone Repair of DNA Double-Strand Breaks. J. Cell. Physiol. *231*, 15–24. https://doi.org/10.1002/jcp.25053.
7. Ratner, E.S., Sartorelli, A.C., and Lin, Z.P. (2012). Poly (ADP-ribose) polymerase inhibitors: on the horizon of tailored and personalized therapies for epithelial ovarian cancer. Curr. Opin. Oncol. *24*, 564–571. https://doi.org/10.1097/CCO.0b013e3283564230.
8. Mansour, W.Y., Schumacher, S., Rosskopf, R., Rhein, T., Schmidt-Petersen, F., Gatzemeier, F., Haag, F., Borgmann, K., Willers, H., and Dahm-Daphi, J. (2008). Hierarchy of nonhomologous end-joining, single-strand annealing and gene conversion at site-directed DNA double-strand breaks. Nucleic Acids Res. *36*, 4088–4098. https://doi.org/10.1093/nar/gkn347.
9. Bhargava, R., Onyango, D.O., and Stark, J.M. (2016). Regulation of Single-Strand Annealing and its Role in Genome Maintenance. Trends Genet. *32*, 566–575. https://doi.org/10.1016/j.tig.2016.06.007.
10. Bai, J.P.F., Alekseyenko, A.V., Statnikov, A., Wang, I.-M., and Wong, P.H. (2013). Strategic applications of gene expression: from drug discovery/development to bedside. AAPS J. *15*, 427–437. https://doi.org/10.1208/s12248-012-9447-1.
11. Kumar Sarvepalli, S. (2015). Deep Learning in Neural Networks: The Science behind an Artificial Brain. https://doi.org/10.13140/RG.2.2.22512.71682.
12. Alzubaidi, L., Zhang, J., Humaidi, A.J., Al-Dujaili, A., Duan, Y., Al-Shamma, O., Santamaría, J., Fadhel, M.A., Al-Amidie, M., and Farhan, L. (2021). Review of deep learning: concepts, CNN architectures, challenges, applications, future directions. J. Big Data *8*, 53. https://doi.org/10.1186/s40537-021-00444-8.
13. Weil, M.K., and Chen, A.P. (2011). PARP inhibitor treatment in ovarian and breast cancer. Curr. Probl. Cancer *35*, 7–50. https://doi.org/10.1016/j.currproblcancer.2010.12.002.
14. Plys, A.J., Rogacheva, M.V., Greene, E.C., and Alani, E. (2012). The unstructured linker arms of Mlh1-Pms1 are important for interactions with DNA during mismatch repair. J. Mol. Biol. *422*, 192–203. https://doi.org/10.1016/j.jmb.2012.05.030.
15. Seol, J.-H., Shim, E.Y., and Lee, S.E. (2018). Microhomology-mediated end joining: Good, bad and ugly. Mutat. Res. *809*, 81–87. https://doi.org/10.1016/j.mrfmmm.2017.07.002.
16. Wang, C., and Lees-Miller, S.P. (2013). Detection and repair of ionizing radiation-induced DNA double strand breaks: new developments in nonhomologous end joining. Int. J. Radiat. Oncol. Biol. Phys. *86*, 440–449. https://doi.org/10.1016/j.ijrobp.2013.01.011.
17. Chiruvella, K.K., Liang, Z., and Wilson, T.E. (2013). Repair of double-strand breaks by end joining. Cold Spring Harbor Perspect. Biol. *5*, a012757. https://doi.org/10.1101/cshperspect.a012757.
18. Moscariello, M., Wieloch, R., Kurosawa, A., Li, F., Adachi, N., Mladenov, E., and Iliakis, G. (2015). Role for Artemis nuclease in the repair of radiation-induced DNA double strand breaks by alternative end joining. DNA Repair *31*, 29–40. https://doi.org/10.1016/j.dnarep.2015.04.004.
19. Beck, C., Boehler, C., Guirouilh Barbat, J., Bonnet, M.-E., Illuzzi, G., Ronde, P., Gauthier, L.R., Magroun, N., Rajendran, A., Lopez, B.S., et al. (2014). PARP3 affects the relative contribution of homologous recombination and nonhomologous end-joining pathways. Nucleic Acids Res. *42*, 5616–5632. https://doi.org/10.1093/nar/gku174.
20. Blasiak, J. (2021). Single-Strand Annealing in Cancer. Int. J. Mol. Sci. *22*, 2167. https://doi.org/10.3390/ijms22042167.
21. Shamanna, R.A., Lu, H., de Freitas, J.K., Tian, J., Croteau, D.L., and Bohr, V.A. (2016). WRN regulates pathway choice between classical and alternative non-homologous end joining. Nat. Commun. *7*, 13785. https://doi.org/10.1038/ncomms13785.
22. Sugawara, N., Goldfarb, T., Studamire, B., Alani, E., and Haber, J.E. (2004). Heteroduplex rejection during single-strand annealing requires Sgs1 helicase and mismatch repair proteins Msh2 and Msh6 but not Pms1. Proc. Natl. Acad. Sci. USA *101*, 9315–9320. https://doi.org/10.1073/pnas.0305749101.
23. Xiong, X., Du, Z., Wang, Y., Feng, Z., Fan, P., Yan, C., Willers, H., and Zhang, J. (2015). 53BP1 promotes microhomology-mediated end-joining in G1-phase cells. Nucleic Acids Res. *43*, 1659–1670. https://doi.org/10.1093/nar/gku1406.
24. Lei, T., Du, S., Peng, Z., and Chen, L. (2022). Multifaceted regulation and functions of 53BP1 in NHEJ-mediated DSB repair (Review). Int. J. Mol. Med. *50*, 90. https://doi.org/10.3892/ijmm.2022.5145.
25. Stefanovie, B., Hengel, S.R., Mlcouskova, J., Prochazkova, J., Spirek, M., Nikulenkov, F., Nemecek, D., Koch, B.G., Bain, F.E., Yu, L., et al. (2020). DSS1 interacts with and stimulates RAD52 to promote the repair of DSBs. Nucleic Acids Res. *48*, 694–708. https://doi.org/10.1093/nar/gkz1052.
26. Chen, R.-C., Dewi, C., Huang, S.-W., and Caraka, R.E. (2020). Selecting critical features for data classification based on machine learning methods. J. Big Data *7*, 52. https://doi.org/10.1186/s40537-020-00327-4.
27. Cancer Genome Atlas Research Network (2011). Integrated genomic analyses of ovarian carcinoma. Nature *474*, 609–615. https://doi.org/10.1038/nature10166.
28. Her, J., and Bunting, S.F. (2018). How cells ensure correct repair of DNA double-strand breaks. J. Biol. Chem. *293*, 10502–10511. https://doi.org/10.1074/jbc.TM118.000371.
29. Uhlen, M., Oksvold, P., Fagerberg, L., Lundberg, E., Jonasson, K., Forsberg, M., Zwahlen, M., Kampf, C., Wester, K., Hober, S., et al. (2010). Towards a knowledge-based

Human Protein Atlas. Nat. Biotechnol. *28*, 1248–1250. https://doi.org/10.1038/nbt1210-1248.

30. Han, J., Ruan, C., Huen, M.S.Y., Wang, J., Xie, A., Fu, C., Liu, T., and Huang, J. (2017). BRCA2 antagonizes classical and alternative nonhomologous end-joining to prevent gross genomic instability. Nat. Commun. *8*, 1470. https://doi.org/10.1038/s41467-017-01759-y.
31. Saha, J., and Davis, A.J. (2016). Unsolved mystery: the role of BRCA1 in DNA end-joining. J. Radiat. Res. *57* (*Suppl 1*), i18–i24. https://doi.org/10.1093/jrr/rrw032.
32. Iwasaki, D., Hayashihara, K., Shima, H., Higashide, M., Terasawa, M., Gasser, S.M., and Shinohara, M. (2016). The MRX Complex Ensures NHEJ Fidelity through Multiple Pathways Including Xrs2-FHA-Dependent Tel1 Activation. PLoS Genet. *12*, e1005942. https://doi.org/10.1371/journal.pgen.1005942.
33. He, D., Li, T., Sheng, M., and Yang, B. (2020). Exonuclease 1 (Exo1) Participates in Mammalian Non-Homologous End Joining and Contributes to Drug Resistance in Ovarian Cancer. Med. Sci. Mon. Int. Med. J. Exp. Clin. Res. *26*, e918751. https://doi.org/10.12659/MSM.918751.
34. Mateos-Gomez, P.A., Gong, F., Nair, N., Miller, K.M., Lazzerini-Denchi, E., and Sfeir, A. (2015). Mammalian polymerase θ promotes alternative NHEJ and suppresses recombination. Nature *518*, 254–257. https://doi.org/10.1038/nature14157.
35. Löbrich, M., and Jeggo, P. (2017). A Process of Resection-Dependent Nonhomologous End Joining Involving the Goddess Artemis. Trends Biochem. Sci. *42*, 690–701. https://doi.org/10.1016/j.tibs.2017.06.011.
36. Layer, J.V., Cleary, J.P., Brown, A.J., Stevenson, K.E., Morrow, S.N., Van Scoyk, A., Blasco, R.B., Karaca, E., Meng, F.-L., Frock, R.L., et al. (2018). Parp3 promotes long-range end joining in murine cells. Proc. Natl. Acad. Sci. USA *115*, 10076–10081. https://doi.org/10.1073/pnas.1801591115.
37. Verma, P., and Greenberg, R.A. (2016). Noncanonical views of homology-directed DNA repair. Genes Dev. *30*, 1138–1154. https://doi.org/10.1101/gad.280545.116.
38. Di Domenico, E.G., Romano, E., Del Porto, P., and Ascenzioni, F. (2014). Multifunctional role of ATM/Tel1 kinase in genome stability: from the DNA damage response to telomere maintenance. BioMed Res. Int. *2014*, 787404. https://doi.org/10.1155/2014/787404.
39. Daley, J.M., and Sung, P. (2013). RIF1 in DNA break repair pathway choice. Mol. Cell *49*, 840–841. https://doi.org/10.1016/j.molcel.2013.02.019.
40. Menon, V., and Povirk, L. (2014). Involvement of p53 in the repair of DNA double strand breaks: multifaceted Roles of p53 in homologous recombination repair (HRR) and non-homologous end joining (NHEJ). Subcell. Biochem. *85*, 321–336. https://doi.org/10.1007/978-94-017-9211-0_17.
41. Bennardo, N., Cheng, A., Huang, N., and Stark, J.M. (2008). Alternative-NHEJ is a mechanistically distinct pathway of mammalian chromosome break repair. PLoS Genet. *4*, e1000110. https://doi.org/10.1371/journal.pgen.1000110.
42. Eckelmann, B.J., Bacolla, A., Wang, H., Ye, Z., Guerrero, E.N., Jiang, W., El-Zein, R., Hegde, M.L., Tomkinson, A.E., Tainer, J.A., and Mitra, S. (2020). XRCC1 promotes replication restart, nascent fork degradation and mutagenic DNA repair in BRCA2-deficient cells. NAR Cancer *2*, zcaa013. https://doi.org/10.1093/narcan/zcaa013.
43. Chang, H.H.Y., Pannunzio, N.R., Adachi, N., and Lieber, M.R. (2017). Non-homologous DNA end joining and alternative pathways to double-strand break repair. Nat. Rev. Mol. Cell Biol. *18*, 495–506. https://doi.org/10.1038/nrm.2017.48.
44. Stinson, B.M., and Loparo, J.J. (2021). Repair of DNA Double-Strand Breaks by the Nonhomologous End Joining Pathway. Annu. Rev. Biochem. *90*, 137–164. https://doi.org/10.1146/annurev-biochem-080320-110356.
45. Ochi, T., Blackford, A.N., Coates, J., Jhujh, S., Mehmood, S., Tamura, N., Travers, J., Wu, Q., Draviam, V.M., Robinson, C.V., et al. (2015). DNA repair. PAXX, a paralog of XRCC4 and XLF, interacts with Ku to promote DNA double-strand break repair. Science *347*, 185–188. https://doi.org/10.1126/science.1261971.
46. Jiang, M., Jia, K., Wang, L., Li, W., Chen, B., Liu, Y., Wang, H., Zhao, S., He, Y., and Zhou, C. (2020). Alterations of DNA damage repair in cancer: from mechanisms to applications. Ann. Transl. Med. *8*, 1685. https://doi.org/10.21037/atm-20-2920.
47. Safran, M., Rosen, N., Twik, M., BarShir, R., Stein, T.I., Dahary, D., Fishilevich, S., and Lancet, D. (2021). The GeneCards Suite. In Practical Guide to Life Science Databases, I. Abugessaisa and T. Kasukawa, eds. (Springer Nature Singapore), pp. 27–56. https://doi.org/10.1007/978-981-16-5812-9_2.
48. Stelzer, G., Rosen, N., Plaschkes, I., Zimmerman, S., Twik, M., Fishilevich, S., Stein, T.I., Nudel, R., Lieder, I., Mazor, Y., et al. (2016). The GeneCards Suite: From Gene Data Mining to Disease Genome Sequence Analyses. CP in Bioinformatics *54*, 1.30.1–1.30.33. https://doi.org/10.1002/cpbi.5.
49. Zhao, S., Ye, Z., and Stanton, R. (2020). Misuse of RPKM or TPM normalization when comparing across samples and sequencing protocols. RNA *26*, 903–909. https://doi.org/10.1261/rna.074922.120.
50. EthanLavi. (2023). GeneExpressionPaperCode. https://doi.org/10.5281/ZENODO.8123030.
51. R Core Team (2022). R: A Language and Environment for Statistical Computing (R Foundation for Statistical Computing). https://www.R-project.org/.
52. Kwak, S.G., and Kim, J.H. (2017). Central limit theorem: the cornerstone of modern statistics. Korean J. Anesthesiol. *70*, 144–156. https://doi.org/10.4097/kjae.2017.70.2.144.
53. Yadav, S., and Shukla, S. (2016). Analysis of k-Fold Cross-Validation over Hold-Out Validation on Colossal Datasets for Quality Classification. In 2016 IEEE 6th International Conference on Advanced Computing (IACC) (IEEE), pp. 78–83. https://doi.org/10.1109/IACC.2016.25.
54. Brodersen, K.H., Ong, C.S., Stephan, K.E., and Buhmann, J.M. (2010). The Balanced Accuracy and Its Posterior Distribution. In 2010 20th International Conference on Pattern Recognition (IEEE), pp. 3121–3124. https://doi.org/10.1109/ICPR.2010.764.
55. Therneau, T., and Atkinson, B. (2022). Rpart: Recursive Partitioning and Regression Trees. R Package version 4.1.16. https://CRAN.R-project.org/package=rpart.
56. Kuhn, M. (2022). Caret: Classification and Regression Training. R package version 6.0-93. https://CRAN.R-project.org/package=caret.
57. Meyer, D., Dimitriadou, E., Hornik, K., Weingessel, A., and Leisch, F. (2022). e1071: Misc Functions of the Department of Statistics, Probability Theory Group (Formerly: E1071), TU Wien. R package version 1.7-12. https://CRAN.R-project.org/package=e1071.
58. Rossum, G. van, and Drake, F.L. (2010). The Python Language Reference Release 3.0.1 [Repr.] (Python Software Foundation).
59. Virtanen, P., Gommers, R., Oliphant, T.E., Haberland, M., Reddy, T., Cournapeau, D., Burovski, E., Peterson, P., Weckesser, W., Bright, J., et al. (2020). SciPy 1.0: fundamental algorithms for scientific computing in Python. Nat. Methods *17*, 261–272. https://doi.org/10.1038/s41592-019-0686-2.
60. Waskom, M. (2021). seaborn: statistical data visualization. JOSS *6*, 3021. https://doi.org/10.21105/joss.03021.
61. Hunter, J.D. (2007). Matplotlib: A 2D Graphics Environment. Comput. Sci. Eng. *9*, 90–95. https://doi.org/10.1109/MCSE.2007.55.
62. Principal Component Analysis Was Performed Using GraphPad Prism Version 9.0.2 for Mac, GraphPad Software, San Diego, California USA, www.graphpad.com.
63. Abadi, M., Agarwal, A., Barham, P., Brevdo, E., Chen, Z., Citro, C., Corrado, G.S., Davis, A., Dean, J., Devin, M., et al. (2016). TensorFlow: Large-Scale Machine Learning on Heterogeneous Distributed Systems.
64. TensorFlow Developers (2022). TensorFlow. https://doi.org/10.5281/ZENODO.6574269.
65. Guyon, I., and Elisseeff, A. (2003). An introduction to variable and feature selection. J. Mach. Learn. Res. *3*, 1157–1182.

STAR★METHODS

KEY RESOURCES TABLE

REAGENT or RESOURCE	SOURCE	IDENTIFIER
Deposited data		
Cleaned data and R and Python code	This paper	RRID:SCR_003193; https://doi.org/10.5281/zenodo.8123030
Software and algorithms		
PCA software	GraphPad, Prism 9.02	www.graphpad.com
Deep learning library	Tensorflow	https://www.tensorflow.org/
Dendrogram generation	SciPy	https://scipy.org/
Clustermap generation	Seaborn	https://seaborn.pydata.org/
Python graphing library	matplotlib	https://matplotlib.org/
Python programming language	Python	https://www.python.org/
Model evaluations	caret	https://cran.r-project.org/package=caret
Decision tree classifier	rpart	https://cran.r-project.org/package=rpart
Naive-bayes and SVM classifiers	e1071	https://cran.r-project.org/package=e1071
R programming language	R Project	https://www.r-project.org/
Other		
Source of data	TCGA Web Program	https://www.cancer.gov/
Protein names to gene names	ProteinAtlas	https://www.proteinatlas.org
Gene names to Ensembl ID	GeneCards	www.genecards.org

RESOURCE AVAILABILITY

Lead contact

Further information and requests for resources, including raw data, should be directed to and will be fulfilled by the lead contact, Z Ping Lin (z.ping.lin@yale.edu).

Materials availability

The source of the data and code in performed analyses are all open-source. The data files used in this study can be obtained through the TCGA web program.

Data and code availability

- The cleaned dataset has been deposited in the Zenodo repository as "data.csv". This paper analyzes existing, publicly available data from the TCGA web program. The accession numbers are listed in the key resources table.
- All original code has been deposited in the Zenodo repository and is publicly available as of the date of publication. Additionally, all 3rd party packages used in the code are open source. DOIs are listed in the key resources table.
- Any additional information required to reanalyze the data can be addressed by the lead contact upon request.

EXPERIMENTAL MODEL AND STUDY PARTICIPANT DETAILS

Ovarian cancer patients

The prognosis and gene expressions of the ovarian cancer patients were extracted from The Cancer Genome Atlas (RRID:SCR_003193).[27] Given the nature of the cancer, the origin of the data was only female patients. The sample of ovarian cancer patients were majority white women (% = 0.86631) around an age mean of 59.58 (sd = 11.3), being classified as high-grade serous ovarian adenocarcinomas.[27] 61.22% of the ovarian cancer patients had a deceased outcome, 26.73% with progression, and 35.29% with recurrence. Lastly, the majority, 72.46% of patients had a FIGO stage as Stage IIIC. The remaining patients made up 15.24% as Stage IV, 4.01% as Stage IIC, 3.74% as Stage IIIB, and 4.55% as the remaining stages.

METHOD DETAILS

Data collection

A set of 48 proteins involved in the NHEJ repair mechanism were identified. Firstly, the NHEJ process will recognize, using the Ku heterodimer, and stabilize the DSB with main NHEJ factors like DNA-PKcs or Ligase IV. From there, Artemis, PNKP, APLF, WRN, and apratoxin, among other proteins, are recruited to bridge the ends and processes them. The next step is litigation of the broken ends via Ligase IV, XLF, and XRCC4.[2] Alternatively, proteins that are involved in the promotion of other pathways, such as HR or SSA, were considered relevant for their antagonistic effect on NHEJ.[28]

Proteins from DNA repair are important to include since the relative activity between pathways could give a quantification of failed NHEJ. As a result, the standard for picking proteins was reported involvement in NHEJ or participation in other pathways with association with NHEJ activity.

Data was scraped from the Human Protein Atlas database to map the of proteins to genes.[29] The final list of genes included *XRCC6, XRCC5, XRCC7, LIG4, LIG3, LIG1, XRCC4, NHEJ1, XRCC1, DCLRE1C, TP53BP1, BRCA1, BRCA2, EXO1, EXD2, POLM, POLL, POLQ, RAD50, MRE11, NBN, TDP1, RBBP8, CTBP1, APLF, PARP1, PARP3, PNKP, APTX, WRN, PAXX, RIF1, RAD52, RAD51, ATM, ATR, TP53, H2AX, ERCC1, ERCC4, RPA1, MSH2, MSH3, RAD1, MSH6, PMS1, MLH1*, and *MLH3*.[2,15–21,23,25,29–46] Following this, the Ensembl IDs, the reference number for each gene, were determined using the Human Gene database, GeneCards.[47,48] FPKM (fragments per kilobase of transcript per million reads mapped)[49] expression levels from 374 ovarian cancer patients and 279 breast cancer patients (653 total) were extracted from the Cancer Genome Atlas (TCGA, December 2020).[27] The other data fields were patient ID, survival status, survival in days, progression status, recurrence status, age, race, ICD10 Code, FIGO stage, neoplasm histologic grade, tumor size, lymphatic invasion status, total dose, number of treatment cycles, treatment start date and end date, therapy type, drug name, and regimen indication. Progression and recurrence status was inferred from treatment regimen indication and were noted to potentially be inaccurate. Some entries were left as null because they were either missing, unavailable, or irrelevant to the study. 52 patients were missing a progression outcome and another 52 were missing a recurrence outcome. More detailed dataset statistics are listed in the Zenodo repository.[50]

The entire set of data was organized into a table and each gene's expression was normalized. The categorical data points of tumor stage, grade, recurrence, and progression were converted to numerical labels and normalized as well. Dataset preparation was conducted using the R programming language.[51]

QUANTIFICATION AND STATISTICAL ANALYSIS

General information

Summary statistics were computed on the dataset using a spreadsheet. The patients used in this analysis were assumed to be independent and randomly selected from the population. Additionally, the central limit theorem justifies the sample being treated as normal.[52] N represents the number of patients used in a given analysis.

10-Fold cross validation

The ovarian cancer patients were reordered randomly and separated into ten distinct sets. These sets were the same in each cross validation conducted. Iterating over each set, one was used as the testing set while the other nine were used as training data.[53] The evaluation metric, balanced accuracy, was then averaged across the ten iterations. Balanced accuracy was chosen because it equally weighted positive and negative predictive strength.[54]

Linear and logistic regression

Linear and logistic regression was chosen to approach modeling starting with low complexity. It also provides clear feature importance. The correlation between each gene expression and survival time was calculated using linear regression (n=374) in R. With regression as the goal, alive patients were given a 20-year survival time and the linear regression model was fitted by minimizing squared residuals for length of survival (Table S1). Logistic regression was included to attempt classification of survival (n=374) (Table 1), progression (n=322) (Table 2), and recurrence (n=322) (Table 3). The positive cases (patient survival, cancer progression, cancer recurrence) were denoted as "1" and all others were "0". The model predicts class probability, in the range 0-1. The threshold for predicting positive or negative was chosen to be 0.5. To evaluate purely the gene capabilities, they were the only predictors used in this analysis. The analysis also produced a coefficient and error for each feature. From this, t-values and p-values were generated. P-values less than 0.1 were chosen as within the threshold for significance in the feature selection, in order to have an adequate subset of data to create models. For the survival models, the corresponding coefficients and p-value of each gene were used to indicate confidence in their positive or negative correlation with survival. The linear regression was evaluated using mean absolute distance, comparing to a baseline of predicting average survival every time. The classifiers were evaluated using balanced accuracy over a 10-fold cross validation.

Decision tree, naive-bayes, support vector machine

To attempt a wider variety of models, a decision tree, a naive-bayes classifier, and a support vector machine were created in R using the rpart, caret, and e1071 packages.[55–57] The intent was to predict survival (n=374), progression (n=322), and recurrence (n=322) using gene expression as the sole predictors. The features selected from the logistic regression analysis were used in training these models. However, an additional trial was conducted to use every gene, testing for relationships missed by the logistic regression feature selection. Balanced accuracy over a 10-fold cross validation were used to evaluate the models and compare them (Table S2). For the naive-bayes, the Laplace parameter was set to 0. For the support vector machines, the linear, polynomial, sigmoid, and radial kernels were all tested to choose the optimal one.

Two sample T-Test

A two sample t-test was performed using R software to compare the average gene expressions of patients over all three binary variables: survival (n=374), progression (n=322), and recurrence (n=322). Looking at each outcome individually, the data was separated into positive and negative sets. The mean and standard deviation of the sets were calculated. The hypothesis for the t-test, whether a positive or negative outcome had higher gene expression, was chosen based on which set had the higher mean. Then, two-sample t-statistics were computed. Finally, a Student's t-distribution was used to calculate the p-value (Table 4). P-values under 0.05 were considered statistically significant.

Baseline accuracy calculation using simulation

With a small sample size, there was concern that the accuracy could be achieved by random variation in the dataset. To further corroborate the accuracy as significant, a simulation was performed in which the logistic regression, decision tree, naive-bayes, and SVM models were re-trained on a randomly generated dataset of the same number of patients and genes. The values drawn followed a normal distribution. Over 100 trials, the balanced accuracy from each model was recorded. The two sample T-Test was also conducted to count the number of significant genes. Lastly, the average and 95% percentile values were calculated.

Hierarchical clustering

Hierarchical clustering was performed to note the relatedness between gene expression variables and survival (n=374). The gene expression variables were isolated to evaluate their predictive capabilities. This analysis was performed on the dataset using SciPy, Matplotlib, and Seaborn software in Python.[58–61] Agglomerative-type clustering was used applying the "ward" linkage method. The results were presented as a heatmap (Figure 2) and dendrogram (Figure 1) to depict the clusters of related genes and ovarian cancer patient outcomes.

Principal component analysis

A principal component analysis (PCA) was performed using the Prism software program (GraphPad) to determine redundancies that can be eliminated in the dataset and the significance of each gene in the dataset (n=374).[62] The gene variables were isolated in this analysis to evaluate them as predictors. The first two principal components were plotted in comparison to survival (Figure S1). In addition, a scree plot (Figure 3) and feature representation plot (Figure S2) was generated.

Neural network

To analyze complex patterns in the data and attempt higher accuracy than current machine learning procedures, a neural network was created. The deep learning approach was implemented using TensorFlow in Python.[63,64] A neural network was designed using two hidden layers, 19 neurons in the first layer and 10 in the second, to predict prognosis. ReLU was used as activation functions for the hidden layers and the sigmoid function was used on output. The training data held the first 80% of the ovarian cancer patients. This training set was used for "Model A". For "Model B", an augmented training group was created by combining breast cancer data with the first training set. "Model B" was only included to predict survival since the recurrence and progression prognoses were unknown for the breast cancer patients. All 274 breast cancer patients were added to help the model predict ovarian cancer prognosis. The validation set held the next 10% of the ovarian cancer patients. The testing set held the remaining 10% of ovarian cancer patients. In predicting progression and recurrence, 52 patients had to be dropped because their clinical outcomes were unknown. This change was reflected in the sizes of each set proportionally (survival had a 300|37|37 split, progression and recurrence had a 258|32|32 split). The models were tested with different hyper-parameters to determine their optimal design, including class weighting to value positive and negative outcomes equally. In addition, feature selection was performed using the forward feature selection technique (Figures 7, 8, and 9). The process begins with no genes. The next-best performing gene was added to the training features iteratively until 35 genes were chosen.[65] Balanced accuracy over three repetitions of 10-fold cross-validation was used for choosing the next gene. The results of this method were graphed using Matplotlib to visualize the increase in best accuracy and average accuracy. Different gene sets were tested to maximize performance. Finally, the models were evaluated on the three binary outcomes: survival (n=374), progression (n=322), and recurrence (n=322), over ten repetitions of 10-fold cross validation. The 10-fold cross-validation was identical to that used in the other machine learning models. Averaged balanced accuracy was used for comparing models. Lastly, Model B was judged against to Model A in three trials: training with all the genes, the best from the forward feature selection, and the genes from the logistic regression feature selection. A bar graph was created using Matplotlib to visualize the differences (Figure S3).

Learning curves

Learning curves were generated for the survival outcome (n=374) with the logistic regression and neural network models. The logistic regression learning curve used the features from the logistic regression feature selection (Figure 7). Two learning curves were made for the neural network, training on the top three (Figure 8) and five (Figure 9) from the forward feature selection. This was done with Matplotlib by plotting training and testing scores when the model learned on differing amounts of examples, incrementing with 1/25 of the training set at a time. The training set consisted of 70% of the ovarian cancer patients and the testing had the remaining 30%. Balanced accuracy was used as the evaluation metric. The logistic regression model was created in R and the neural network was built in Python. The neural network scores for each training set size were averaged over six repetitions.